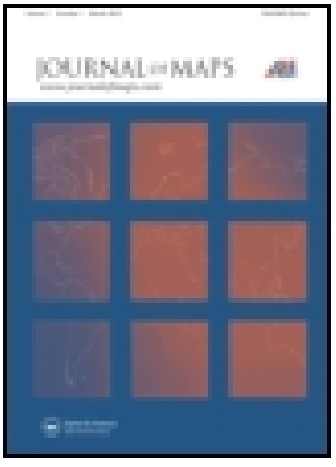

Journal of Maps
Publication details, including instructions for authors and subscription information:
http://www.tandfonline.com/loi/tjom20

Structural map of Variscan northern Sardinia (Italy)

Leonardo Casini[a], Stefano Cuccuru[a], Matteo Maino[b], Giacomo Oggiano[a], Antonio Puccini[a] & Philippe Rossi[c]
[a] DipNeT, University of Sassari, Sassari, Italy
[b] DiSTA, University of Pavia, Pavia, Italy
[c] BRGM, Orléans Cedex 2, France
Published online: 03 Jul 2014.

To cite this article: Leonardo Casini, Stefano Cuccuru, Matteo Maino, Giacomo Oggiano, Antonio Puccini & Philippe Rossi (2014): Structural map of Variscan northern Sardinia (Italy), Journal of Maps, DOI: 10.1080/17445647.2014.936914

To link to this article: http://dx.doi.org/10.1080/17445647.2014.936914

Journal of Maps, 2014
http://dx.doi.org/10.1080/17445647.2014.936914

SCIENCE

Structural map of Variscan northern Sardinia (Italy)

Leonardo Casini[a*], Stefano Cuccuru[a], Matteo Maino[b], Giacomo Oggiano[a], Antonio Puccini[a] and Philippe Rossi[c]

[a]*DipNeT, University of Sassari, Sassari, Italy;* [b]*DiSTA, University of Pavia, Pavia, Italy;* [c]*BRGM, Orléans Cedex 2, France*

(*Received 27 February 2014; resubmitted 29 April 2014; accepted 21 May 2014*)

In this paper, we present a geological structural map (1:100,000 scale, ~2300 km^2 surface area) of the Variscan basement of northern Sardinia. The map integrates field structural analysis, extensive gamma-ray spectrometry, and high-resolution ELA-ICP-MS U/Th-Pb zircon and monazite dating. A set of 10 samples of granitic rocks collected from different plutons were characterized for their crystallization age. This provided an accurate timing of magmatic events related to the development of the Corsica-Sardinia Batholith. The structural map, complemented with geochronological results represents a benchmark for future studies on Variscan geodynamics.

Keywords: Variscan; Corsica-Sardinia Batholith; pluton; shear zones; zircon dating

1. Introduction

The Variscan belt of southern Europe includes several Late Mississippian to Early Permian magmatic provinces broadly related to post-collisional extension and thermal re-equilibration of the crust (Casini, Puccini, Cuccuru, Maino, & Oggiano, 2013; Gébelin, Roger, & Brunel, 2009; Vilà, Fernández, & Jiménez-Munt, 2010). Most Carboniferous plutons emplaced within late-orogenic strike-slip shear zones relate to the late Variscan phase of wrench tectonics (Matte, 2001). This recognized structural control motivated geologists to improve their knowledge about the geometry and timing of different plutons in relation to major orogenic events. Work has included detailed structural maps of Variscan batholiths that have been coupled to high-resolution geochronological studies in the French Massif Central (Faure, Cocherie, Mézème, Charles, & Rossi, 2010; Gébelin et al., 2009), External Crystalline Massifs on the western Alps (Rubatto, Ferrando, Compagnoni, & Lombardo, 2010), the Pyrenean region (Liesa et al., 2011; Vilà et al., 2010) and the Corsica-Sardinia block (Casini, Cuccuru, Maino, Oggiano, & Tiepolo, 2012; Gattacceca et al., 2004; Gébelin et al., 2009; Rossi & Cocherie, 1991). However, recent work on the Sardinian part of the Corsica-Sardinia Batholith have focused on petrological aspects related to the origin of melts (Cruciani, Franceschelli, Jung, Puxeddu, & Utzeri, 2008; Ferré & Leake, 2001; Gaggero, Oggiano, Buzzi, Slejko, & Cortesogno, 2007; Macera, Di Pisa, & Gasperini, 2011). In this study, we present the first structural map (Main Map) of the Variscan basement of north Sardinia

*Corresponding author. Email: casini@uniss.it

(Italy), including fine detail of the internal structure of the Corsica-Sardinia Batholith (C-SB) (Ferré & Leake, 2001; Rossi & Cocherie, 1991). Mapping of metamorphic complexes and late-orogenic plutons was primarily based on field structural analysis at 1:10,000 scale and remote sensing. The results have been strengthened by high-resolution ELA-ICP-MS U-Pb zircon dating of selected samples, and extensive γ-ray spectrometric surveys on granitic massifs.

2. Geological setting

The Variscan belt results from the successive welding of Laurussia, Avalonia and the Armorican terranes against Gondwana during Devonian-Carboniferous times (Matte, 2001). Devonian subduction was followed by oblique collision of the northern Gondwana margin against Armorica in Famennian – Tournaisian times (Edel, Schulmann, Skrzypek, & Cocherie, 2013; Matte, 2001). The final convergence between the continental blocks was characterized by the development of a wide network of lithospheric strike-slip shear zones, which accommodated the northeastward displacement of Laurussia and Avalonia relative to stable Gondwana from late Visean to Early Permian (Faure, Lardeaux, & Ledru, 2009; Gutiérrez-Alonso et al., 2008; Muttoni, Kent, & Channell, 1996). The pre-Mesozoic basement of north Sardinia is a section of the Variscan orogen equivalent to the Moldanubian domain (Figure 1) of central Europe (Edel et al., 2013; Matte, 2001; Rossi, Oggiano, & Cocherie, 2009). Metamorphic units consist of an Upper Migmatitic Complex (UMC), made of metatexites, diatexites, and migmatitic orthogneisses of Ordovician protholith age (Buzzi, Gaggero, & Oggiano, 2008; Casini et al., 2012; Oggiano, Gaggero, Funedda, Buzzi, & Tiepolo, 2010), and a Lower Metamorphic Complex (LMC), made of

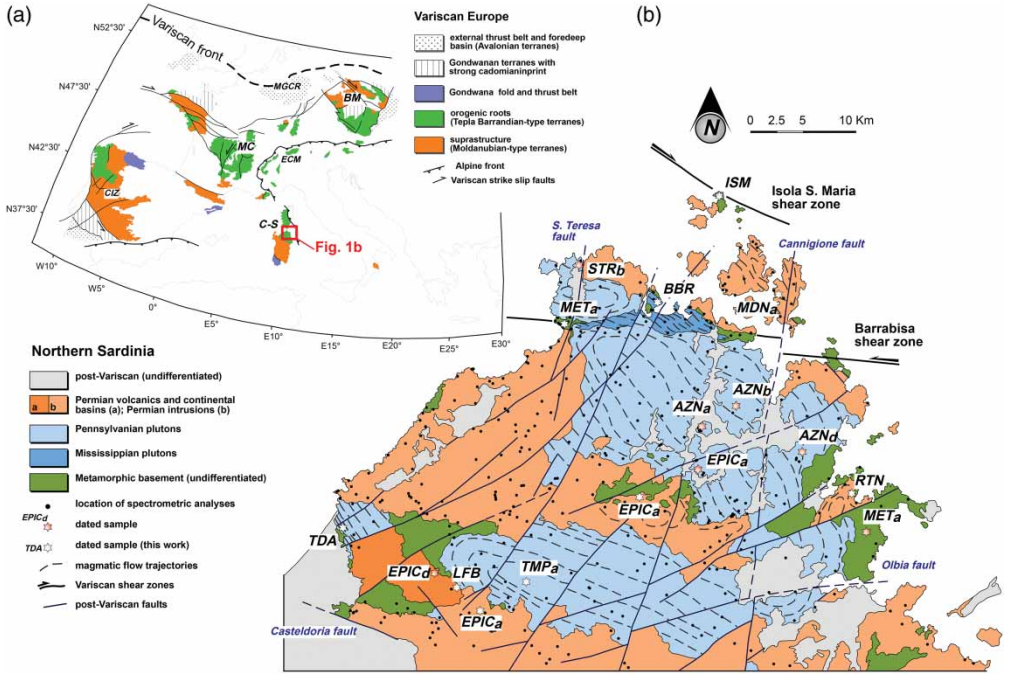

Figure 1. (a) structural scheme of Variscan Europe: CIZ, Central Iberian Zone; MC, French Massif Central; ECM, External Crystalline Massif of the Alps; BM, Bohemian Massif; MGCR, Mid-German Crystalline Ridge; C-S, Corsica-Sardinia Massif. The main late-Variscan shear zones and the Alpine front are also indicated. (b) Tectonic scheme of northern Sardinia.

paragneisses, micaschists, quartzites and subordinate amphibolite boudins (Cappelli et al., 1991; Carmignani et al., 1994).The Visean collisional evolution is testified by exhumation of HP rocks and southward thrusting of UMC onto LMC. The phase of shortening is associated with near-isothermal decompression and partial melting of UMC in the kyanite stability field (Ferrara, Ricci, & Rita, 1978; Giacomini, Bomparola, & Ghezzo, 2005). The limit between UMC and the lower grade, mainly amphibolitic, LMC, is marked by a 1–3 km-thick lithospheric shear zone known as the Posada-Asinara Line (PAL) (Cappelli et al., 1991). Metamorphic rocks are widely intruded by a network of late Variscan plutons belonging to the Corsica-Sardinia Batholith (Rossi & Cocherie, 1991). Zircon dating indicates that plutons were episodically emplaced from Late Mississippian to Permian, during post-collisional extension and exhumation of the crust (Casini et al., 2013; Paquette, Ménot, Pin, & Orsini, 2003).

3. Methods

3.1. *Remote sensing*

Image analysis provided a preliminary inspection of the geometry of faults and principal magmatic contacts in northern Sardinia. A digital elevation model (DEM) of northern Sardinia was created from a mosaic of 1:10,000 topographic maps. The DEM was integrated with georeferenced high-resolution aerial orthophotos (property of Regione Autonoma della Sardegna) and IKONOS 2005 satellite images. Detailed information about the spatial resolution and accuracy of the images can be found in (Virdis, Oggiano, & Disperati, 2012). The results were processed using Matlab to extract significant geomorphological features related to tectonic structures, such as major faults, joints networks, and lithologic contacts within granitic outcrops. The algorithm consists of a pre-processing routine that converts true color RGB images into grayscale images by calculating the luminance (Y) component as the weighted sum of the three color channels (R, G and B), as $Y = 0.299\mathrm{R} + 0.587\mathrm{G} + 0.114\mathrm{B}$. User-defined features were identified using a semi-automatic pattern recognition routine based on the Hit-or-Miss Transform method for grayscale images (Soille, 1999).

3.2. *Field structural analysis*

The geometry of plutons and their emplacement-related fabric were investigated by structural analysis (Vernon, Johnson, & Melis, 2004). The magmatic flow trajectories have been constrained measuring the shape preferred orientation of various flow markers, such as: (i) metamorphic xenoliths, (ii) large, idiomorphic k-feldspar phenocrysts, (iii) micro-granular mafic enclaves, (iv) micro-granitoid batches, (v) schlieren of biotite, and (vi) pegmatite or aplite veins. Except for fine-grained Permian leuco-monzogranites, that lack any consistent flow marker, several measurements have been performed in all plutons to portray the fine detail of the magmatic structure with an optimal statistical coverage.

3.3. *Gamma-ray spectrometry measurements*

Magmatic rocks and metamorphic high-grade rocks have been characterized for their U, Th and K composition (Puccini et al., 2014). The portable gamma-ray spectrometer adopted for this study consists of an NaI(Tl) single crystal with a cubic shape ($10.2 \times 10.2 \times 10.2\ \mathrm{cm}^3$) and energy resolution of 7.3% at 662 keV (^{137}Cs) and 5.2% at 1172 and 1332 keV (^{60}Co). The crystal is optically coupled with an integrated photomultiplier tube consisting of bias supply, preamplifier and digital multichannel analyzer. The device is controlled by a portable computer that allows

processing of the raw spectrum in real time, determining the concentration of both ^{235,238}U ^{232}Th [ppm], and ^{40}K [%] directly in the field using the jRadview software package (Caciolli et al., 2012). The analysis is performed over the full spectrum using a non-negative least squares (FSA-NNLS) constraint; each spectrum is reconstructed from a linear combination of the standard spectra for ^{238}U, ^{232}Th, ^{40}K, ^{137}Cs and the background radiation. The concentration of $^{235,\ 238}$U and ^{232}Th are estimated by ^{214}Bi and ^{208}Tl decay, under the assumption that the uranium and thorium decay series are in secular equilibrium. In 396 measurements on different Variscan rocks of North Sardinia, statistical uncertainties were below 1.5% for ^{40}K and about 3% for ^{235,238}U and ^{232}Th, respectively (Figure 2).

3.4. *Geochronology*

In order to implement the geochronological constraints of the granites history, 10 representative samples of magmatic and metamorphic rocks exposed in northern Sardinia were selected for *in-situ* U-Pb zircon dating (Table 1). Mineral separation was carried out using conventional methods (vibrating table, magnetic separation and heavy liquids). Crystals without fractures, visible inclusions, and compositional zonations were identified by backscattered electron (BSE) and cathodoluminescence (CL) analysis with a Scanning Electron Microscope (SEM-JEOL JXA840). Suitable zircon grains were hand-picked, mounted in epoxy resin and polished using 0.25 μm diamond paste. The ^{202}Hg, ^{204}(Pb + Hg), $^{206,\ 207,\ 208}$Pb, ^{232}Th and ^{238}U isotopic compositions were determined with excimer laser ablation (ELA)-ICP-MS at the CNR - IGG - Unità di Pavia. The laser ablation instrument consists of an ArFexcimer laser microprobe at 193 nm (Geolas200Q-Microlas) and a high-resolution sector field ICP-MS. The instrumental and laser-induced U–Pb fractionations were corrected adopting the 1065 Ma 91500 zircon (Wiedenbeck et al., 1995) as external standard. The spot size was set to 20 μm and laser fluence to 12 Jcm^{-2}. Approximately 60s of background and at least 30s of ablation signal were acquired in all analyses. Data reduction was performed using the Glitter software package (Van Achterberg, Ryan, Jackson, & Griffin, 2001). The reproducibility

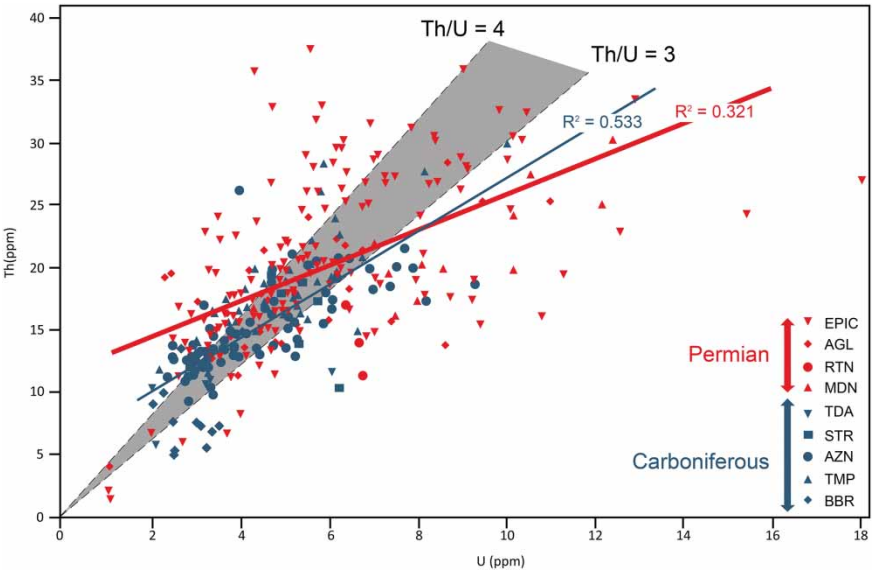

Figure 2. Variation of Th/U ratio in Variscan plutons of northern Sardinia; blue and red symbols identify Carboniferous and Permian plutons, respectively.

Table 1. Geochronological contraints.

Coordinates	Label	Rock type	Age [Ma]	method	Interpretation	References
41.007559 9.260120	EPICa (sample BO2)	Quarzodiorite	285.8 ± 1.9	U-Pb zircon, (ELA) ICP MS	crystallization	this work
41.043367 9.357653	EPICa	Granodiorite	286.5 ± 4.3	U-Pb zircon	crystallization	(Gaggero et al., 2007)
40.892815 9.054167	EPICa (sample SANT3)	Granodiorite	288.3 ± 2.5	U-Pb zircon, (ELA) ICP MS	crystallization	this work
41.004844 9.549775	RTN	Granodiorite	290 ± 2	U-Pb zircon, (ELA) ICP MS	crystallization	this work
40.917599 9.031947	LFB	Conglomerate	294	U-Pb zircon, (ELA) ICP MS	depositional age	this work
41.215338 9.452620	MDNa	Monzo-granodiorite	294 ± 4	U-Pb zircon, (ELA) ICP MS	crystallization	this work
40.971857 8.894967	TDA	Granodiorite	300.1 ± 6.1	U-Pb zircon, (ELA) ICP MS	crystallization	this work
41.239401 9.196811	STRb	Monzogranite	307 +5/−2	U-Pb zircon	crystallization	(Oggiano et al., 2005)
41.046300 9.477080	AZNd	Leucomonzogranite	307.6 ± 3.5	U-Pb zircon, (ELA) ICP MS	crystallization	(Casini et al., 2012)
41.078103 9.395170	AZNb	Monzogranite	311 +6/−4 Ma	U-Pb zircon	crystallization	(Oggiano et al., 2005)
40.905746 9.150176	TMPa	Monzogranite	316 ± 2.3	U-Pb zircon, (ELA) ICP MS	crystallization	this work
41.073714 9.351474	AZNa	Granodiorite	320 ± 10	U-Pb zircon, (ELA) ICP MS	crystallization	(Casini et al., 2012)
41.201246 9.291145	BBR	Granodiorite	313.4 ± 5.1	U-Pb monazite, (ELA) ICP MS	crystallization	this work
41.304215 9.377360	ISM	Granodiorite	321.8 ± 8.3	U-Pb zircon, (ELA) ICP MS	crystallization	this work
40.971535 9.566708	METa	Eclogite	351.7 ± 2.9	U-Pb zircon	metamorphism	(Giacomini et al., 2005)
41.17857 9.172581	METa	Orthogneiss	480.7 ± 2.9	U-Pb zircon, (ELA) ICP MS	protholith	this work
40.916641 9.019022	EPICd	Rhyolite	288 ± 11 Ma	Rb/Sr WR	crystallization	(Del Moro et al., 1996)

of the standards was propagated to all determinations according to the equation of Horstwood, Foster, Parrish, Noble, and Nowell (2003); after this procedure, analyses were considered accurate within quoted errors. A 295 Ma 02123 zircon (Ketchum, Jackson, Culshaw, & Barr, 2001) was analyzed during each run for quality control, yielding 1.7% (2 sigma) mean accuracy. The isotopic ages were calculated using the concordia method (Wetherill, 1956).

4. Structure and geochronology of the Corsica-Sardinia Batholith

The structural mapping of northern Sardinia shows fragments of a Variscan high-grade, mainly migmatitic, metamorphic basement intruded by the Corsica-Sardinia Batholith (C-SB). Anatexis and southward thrusting of UMC onto the LMC occurred in Late Devonian – Early Visean (351.7 ± 2.9 Ma, Table 1), typical of crustal melting in the Moldanubian domain of central Europe (Faure et al., 2010). The oldest magmatic complexes in the Sardinian part of C-SB are indicated in the map as Barrabisa (BBR) and Isola di S. Maria (ISM) plutons. They consist of dyke-shaped, S- to I-type, strongly foliated peraluminous monzogranites and granodiorites emplaced between 15–20 km of depth within E-W and NW-SE ductile shear zones rooted in a granulitic lower crust (Casini, 2012; Casini et al., 2012, 2013). The early U2 plutons show systematically moderate to absent grain-size reduction towards the migmatitic host rock and preserve a well-developed magmatic foliation almost parallel to the fabric of migmatites (Figure 3). All these features indicate that the contacts between the host migmatites and these plutons were plastic at the time of emplacement (Casini et al., 2012), which is consistent with the inferred emplacement depths (Figure 3). U/Th-Pb zircon and monazite dating provided two similar crystallization ages of 321.2 ± 8.3 Ma (ISM, zircon) and 313.4 ± 5.1 Ma (BBR, monazite), respectively (Table 1). The early granodiorites were successively intruded by larger, sill-shaped, metaluminous to slightly peraluminous monzogranitic plutons of Early Pennsylvanian to Early Permian age (320–290 Ma), indicated on the map as Tempio (TMP_a, 316.8 ± 2.3 Ma), Arzachena (AZN_a, 320 ± 10; AZN_b, 311 ± 5 Ma; AZN_d, 308.1 ± 3.8), S. Teresa (STR_b, 307 ± 4 Ma), La Maddalena (MDN_a, 294 ± 4 Ma), Porto Rotondo (RTN, 290 ± 3 Ma), Trinità d'Agultu (TDA, 300.1 ± 6.1 Ma) and Aglientu (AGL, undated). In the mapped area, the fabric of these plutons is overall flat or gently dipping to the NE in contrast to the vertical structure of the BBR and ISM plutons (Figure 3). This difference indicates a transition from strike-slip tectonics, typical of Variscides in Pennsylvanian times, to distributed horizontal flow probably related to sudden injection of large volumes of melt (Casini et al., 2012).

The younger magmatic complex (~290–270 Ma) is labeled on the map as the Early Permian Igneous Complex (EPIC). It consists of several compositionally heterogeneous plutons and subvolcanic complexes emplaced within NE-SW tensional fractures that collectively form large E-W belts (Figure 1). The relatively more mafic terms ($EPIC_a$) such as gabbro and granodiorite gave consistent ages ranging from about 290 to about 285 Ma (sample SANT3: 288.3 ± 2.5 Ma; sample BO2: 285.8 ± 1.9 Ma). EPIC is formed by the mixing of mafic, poorly evolved, subalkaline to alkaline melts and crustal melts (Gaggero et al., 2007; Renna, Tribuzio, & Tiepolo, 2006). Brittle contacts decorated by magmatic breccias can be observed around the mafic bodies (Figure 3); therefore, it is likely that part of the crustal component derived from re-melting of the pre-Sakmarian plutons. The results of gamma-ray analysis support this interpretation as Late Carboniferous plutons have a distinctive Th/U ratio mostly in the 3 to 4 range, whereas Early Permian granites, including EPIC, show a much larger spread of values (Figure 2).

An Early Permian continental basin, indicated as the Lu Falzu Basin on the map (LFB), is distinguished in the uppermost section of EPIC, beneath a rhyolitic volcanic sequence dated at 288 ± 11 Ma by the Rb/Sr whole rock isochron method (Del Moro, Di Pisa, & Oggiano, 1996). This is a narrow transtensional basin filled by a thick (~700 mt) sequence of

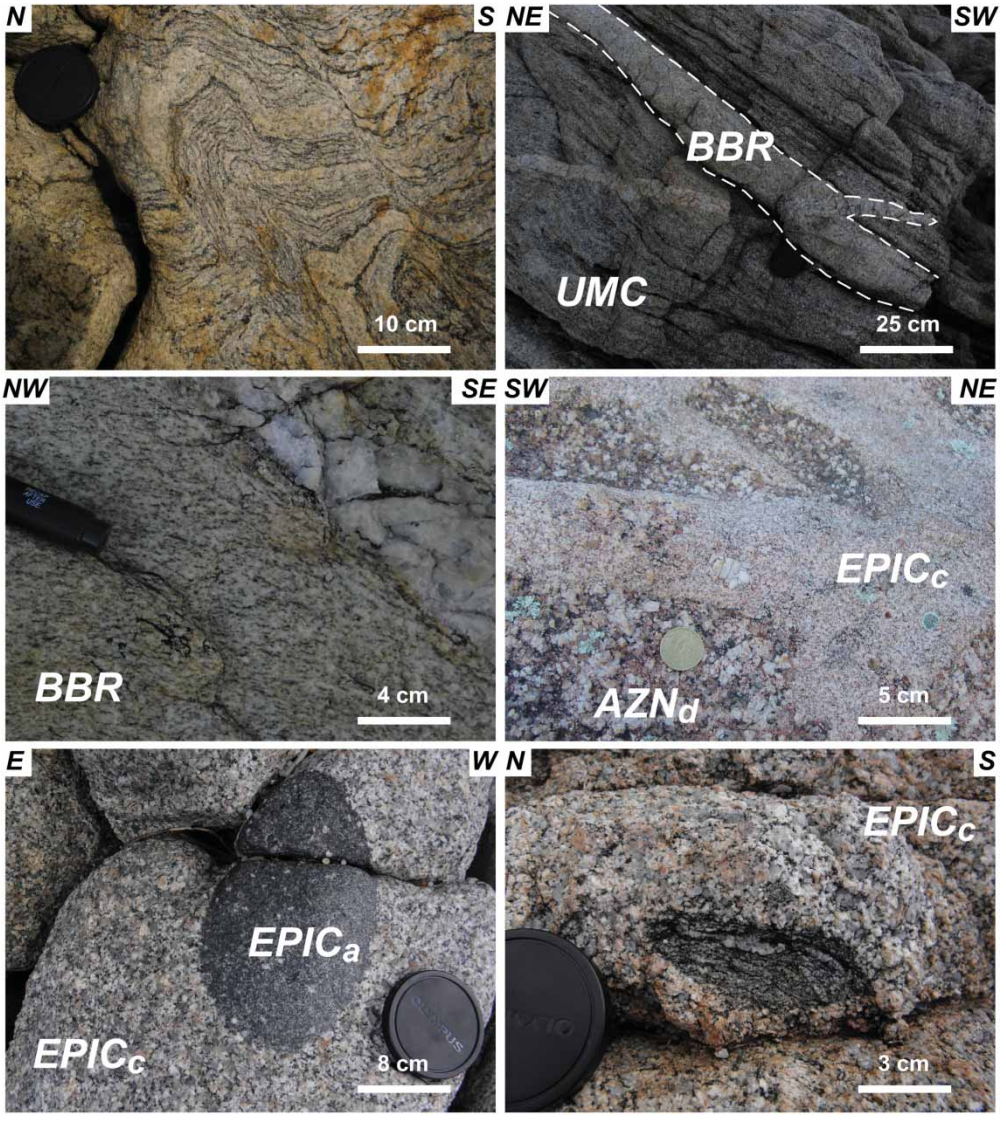

Figure 3. (a) migmatitic orthogneiss derived from Ordovician protholith; (b) ductile contact between late Mississippian granodiorite (BBR) and metatexite (UMC); (c) detail of magmatic to sub-magmatic foliation in BBR granodiorite; (d) brittle, 'cold' contact between a Permian fine-grained monzogranite ($EPIC_c$) and the southern margin of the Arzachena pluton (AZN_d); (e) micro-granular, mafic enclave ($EPIC_a$) enclosed within a coeval Permian sub-alkaline granite ($EPIC_c$); f) metamorphic xenolith partly trapped within Permian monzogranite ($EPIC_c$).

conglomerates, muddy siltites and black quartzites. The sediments were accumulated along a NNW-SSE fault active since at 294 Ma, as indicated by the youngest ages of detrital zircons in the basal conglomerate (Table 1). The lower part of LFB in contact with a gabbroic complex associated with EPIC recorded HT-LP contact metamorphism at about 285 Ma. Finally, all lithostratigraphic units of post-Permian age, including Tethysian carbonate platforms and Eocene to Quaternary volcanic-sedimentary cover, have been grouped together for simplicity.

4.1. Post-Variscan brittle tectonics

The map shows several mainly NW-SE dextral and NE-SW sinistral strike-slip faults cutting across northern Sardinia. These structures displace the pre-Carboniferous metamorphic units and all plutons of the C-SB, including the youngest Permian complexes collectively indicated as EPIC. Therefore, in the absence of high-resolution geochronologic constraints, faulting is inferred to be Late-Carboniferous to Early Permian and possibly related to the large clockwise rotation of the Corsica-Sardinia block in late Variscan times (Edel, Casini, Oggiano, Rossi, & Schulmann, 2014). The faults characterized by sinistral kinematic and NE to ENE direction entangle the Mesozoic-Cenozoic sedimentary and volcanic sequences, generating either positive flower structures or strike-slip basins corresponding to restraining or releasing bends respectively (Carmignani et al., 1994). The age of syntectonic sediments indicates that most of these late Variscan faults were reactivated in Oligocene to Miocene times (Carmignani et al., 1995), during the collision between the Corsica-Sardinia block and Adria (Carmignani, Funedda, Oggiano, & Pasci, 2004; Oggiano, Funedda, Carmignani, & Pasci, 2009). The major structures, such as the Cannigione and Olbia faults (Figure 1), are traceable for several tens of kilometers and show up to 5–7 km of horizontal offset, bridging different plutons and generating a complex mosaic pattern.

5. Conclusions

This paper presents the first detailed structural map of the Variscan basement of north Sardinia (Italy), including the southern part of the Corsica-Sardinia Batholith. High-resolution zircon dating of 10 selected samples of late Variscan plutons, together with published geochronological constraints, evidence two principal magmatic domains. The first consists of pre-Sakmarian peraluminous to metaluminous S- to I-type granites injected within E-W and NNW-SSE shear zones. The younger plutons (~290–275 Ma) are generally A- to S-type leuco-monzogranites emplaced within NE-SW dilatant zones. These latter massifs are systematically associated with sub-alkaline to alkaline mafic complexes (~288–284 Ma) composed of gabbros and diorites.

Software

The geological map was digitized using Esri ArcGIS 9.3. Google Earth and Matlab were used for remote sensing analysis. Field spectrometric analysis was performed using jRadview (Caciolli et al., 2012). The isotopic composition of zircon and monazite grains was analyzed using the Glitter package (Van Achterberg et al., 2001).

References

Buzzi, L., Gaggero, L., & Oggiano, G. (2008). The Santa Giusta ignimbrite (NW Sardinia): A clue for the magmatic, structural and sedimentary evolution of a Variscan segment between Early Permian and Triassic. *Bollettino della Societa Geologica Italiana*, *127*(3), 683–695.

Caciolli, A., Baldoncini, M., Bezzon, G. P., Broggini, C., Buso, G. P., Callegari, I., ... Xhixha, G. (2012). A new FSA approach for in situ γ ray spectroscopy. *Science of The Total Environment*, *414*, 639–645. doi: 10.1016/j.scitotenv.2011.10.071

Cappelli, B., Carmignani, L., Castorina, F., Di Pisa, A., Oggiano, G., & Petrini, R. (1991). A Hercynian suture zone in Sardinia: Geological and geochemical evidence. *Geodinamica Acta*, *5*(1–2), 101–118.

Carmignani, L., Carosi, R., Di Pisa, A., Gattiglio, M., Musumeci, G., Oggiano, G., & Pertusati, P. C. (1994). The Hercynian chain in Sardinia (Italy). *Geodinamica Acta*, *7*(1), 31–47.

Carmignani, L., Decandia, F. A., Disperati, L., Fantozzi, P. L., Lazzarotto, A., Liotta, D., & Oggiano, G. (1995). Relationships between the Tertiary structural evolution of the Sardinia-Corsica-Provencal domain and the northern Apennines. *Terra Nova*, *7*(2), 128–137.

Carmignani, L., Funedda, A., Oggiano, G., & Pasci, S. (2004). Tectono-sedimentary evolution of southwest Sardinia in the Paleogene: Pyrenaic or apenninic dynamic? *Geodinamica Acta*, *17*(4), 275–287.

Casini, L. (2012). A MATLAB-derived software (geothermMOD1.2) for one-dimensional thermal modeling, and its application to the Corsica-Sardinia batholith. *Computers & Geosciences*, *45*, 82–86. doi: 10.1016/j.cageo.2011.10.020

Casini, L., Cuccuru, S., Maino, M., Oggiano, G., & Tiepolo, M. (2012). Emplacement of the Arzachena Pluton (Corsica–Sardinia Batholith) and the geodynamics of incoming Pangaea. *Tectonophysics*, *544-545*, 31–49. doi: 10.1016/j.tecto.2012.03.028

Casini, L., Puccini, A., Cuccuru, S., Maino, M., & Oggiano, G. (2013). GEOTHERM: A finite difference code for testing metamorphic P–T–t paths and tectonic models. *Computers & Geosciences*, *59*, 171–180. doi: 10.1016/j.cageo.2013.05.017

Cruciani, G., Franceschelli, M., Jung, S., Puxeddu, M., & Utzeri, D. (2008). Amphibole-bearing migmatites from the Variscan Belt of NE Sardinia, Italy: Partial melting of mid-Ordovician igneous sources. *Lithos*, *105*(3–4), 208–224. doi: 10.1016/j.lithos.2008.03.009

Del Moro, A., Di Pisa, A., & Oggiano, G. (1996). Relationships between an Autunian volcano-sedimentary succession and the Tempio massif granites (Northern Sardinia): Geochronological and field constraints. *Plinius*, *16*, 94–95.

Edel, J. B., Casini, L., Oggiano, G., Rossi, P., & Schulmann, K. (2014). Early Permian 90 clockwise rotation of the Maures-Esterel-Corsica-Sardinia block confirmed by new palaeomagnetic data and followed by a Triassic 60 clockwise rotation. London: Geological Society, Special Publications. doi: 10.1144/sp405.10

Edel, J. B., Schulmann, K., Skrzypek, E., & Cocherie, A. (2013). Tectonic evolution of the European Variscan belt constrained by palaeomagnetic, structural and anisotropy of magnetic susceptibility data from the Northern Vosges magmatic arc (eastern France). *Journal of the Geological Society*, *170*(5), 785–804. doi: 10.1144/jgs2011-138

Faure, M., Cocherie, A., Mézème, E. B., Charles, N., & Rossi, P. (2010). Middle Carboniferous crustal melting in the Variscan Belt: New insights from U–Th–Pbtot. monazite and U–Pb zircon ages of the Montagne Noire Axial Zone (southern French Massif Central). *Gondwana Research*, *18*(4), 653–673. doi: 10.1016/j.gr.2010.02.005

Faure, M., Lardeaux, J.-M., & Ledru, P. (2009). A review of the pre-Permian geology of the Variscan French Massif Central. *Comptes Rendus Geoscience*, *341*(2–3), 202–213. doi: 10.1016/j.crte.2008.12.001

Ferrara, G., Ricci, C. A., & Rita, F. (1978). Isotopic ages and tectono-metamorphic history of the metamorphic basement of North-Eastern Sardinia. *Contributions to Mineralogy and Petrology*, *68*(1), 99–106. doi: 10.1007/bf00375451

Ferré, E. C., & Leake, B. E. (2001). Geodynamic significance of early orogenic high-K crustal and mantle melts: Example of the Corsica Batholith. *Lithos*, *59*(1–2), 47–67. doi: 10.1016/s0024-4937(01)00060-3

Gaggero, L., Oggiano, G., Buzzi, L., Slejko, F. F., & Cortesogno, L. (2007). Post-variscan mafic dikes from the late orogenic collapse to the Tethyan rift: Evidence from Sardinia. *Ofioliti*, *32*(1), 15–37.

Gattacceca, J., Orsini, J. B., Bellot, J. P., Henry, B., Rochette, P., Rossi, P., & Cherchi, G. (2004). Magnetic fabric of granitoids from Southern Corsica and Northern Sardinia and implications for Late Hercynian tectonic setting. *Journal of the Geological Society*, *161*(2), 277–289. doi: 10.1144/0016-764903-115

Gébelin, A., Roger, F., & Brunel, M. (2009). Syntectonic crustal melting and high-grade metamorphism in a transpressional regime, Variscan Massif Central, France. *Tectonophysics*, *477*(3–4), 229–243. doi: 10.1016/j.tecto.2009.03.022

Giacomini, F., Bomparola, R. M., & Ghezzo, C. (2005). Petrology and geochronology of metabasites with eclogite facies relics from NE Sardinia: Constraints for the Palaeozoic evolution of Southern Europe. *Lithos*, *82*(1-2), 221–248. doi: 10.1016/j.lithos.2004.12.013

Gutiérrez-Alonso, G., Fernández-Suárez, J., Weil, A. B., Brendan Murphy, J., Damian Nance, R., Corfú, F., & Johnston, S. T. (2008). Self-subduction of the Pangaean global plate. *Nature Geoscience*, *1*(8), 549–553. doi: 10.1038/ngeo250

Horstwood, M. S. A., Foster, G. L., Parrish, R. R., Noble, S. R., & Nowell, G. M. (2003). Common-Pb corrected in situ U-Pb accessory mineral geochronology by LA-MC-ICP-MS. *Journal of Analytical Atomic Spectrometry*, *18*(8), 837–846. doi: 10.1039/b304365 g

Ketchum, J. W. F., Jackson, S. E., Culshaw, N. G., & Barr, S. M. (2001). Depositional and tectonic setting of the Paleoproterozoic Lower Aillik Group, Makkovik Province, Canada: Evolution of a passive margin-foredeep sequence based on petrochemistry and U–Pb (TIMS and LAM-ICP-MS) geochronology. *Precambrian Research*, *105*(2-4), 331–356. doi: 10.1016/s0301-9268(00)00118-2

Liesa, M., Carreras, J., Castiñeiras, P., Casas, J. M., Navidad, M., & Vilà, M. (2011). U-Pb zircon age of Ordovician magmatism in the Albera Massif (Eastern Pyrenees). *Geologica Acta*, *9*(1), 93–101. doi: 10.1344/105.000001651

Macera, P., Di Pisa, A., & Gasperini, D. (2011). Geochemical and Sr–Nd isotope disequilibria during multi-stage anatexis in a metasedimentary Hercynian crust. *European Journal of Mineralogy*, *23*(2), 207–222. doi: 10.1127/0935-1221/2011/0023-2091

Matte, P. (2001). The Variscan collage and orogeny (480-290 Ma) and the tectonic definition of the Armorica microplate: A review. *Terra Nova*, *13*(2), 122–128. doi: 10.1046/j.1365-3121.2001.00327.x

Muttoni, G., Kent, D. V., & Channell, J. E. T. (1996). Evolution of Pangea: Paleomagnetic constraints from the Southern Alps, Italy. *Earth and Planetary Science Letters*, *140*(1-4), 97–112. doi: 10.1016/0012-821x(96)00038-6

Oggiano, G., Cherchi, G.P., Aversano, A., Di Pisa, A., Ulzega, A., Orrù, P., & Pintus, C. (2005). Note Illustrative della Carta Geologica d'Italia alla scala 1:50000. Foglio 428, Arzachena, Firenze.

Oggiano, G., Funedda, A., Carmignani, L., & Pasci, S. (2009). The Sardinia-Corsica microplate and its role in the Northern Apennine Geodynamics: New insights from the Tertiary intraplate strike-slip tectonics of Sardinia. *Bollettino della Societa Geologica Italiana*, *128*(2), 527–539.

Oggiano, G., Gaggero, L., Funedda, A., Buzzi, L., & Tiepolo, M. (2010). Multiple early Paleozoic volcanic events at the northern Gondwana margin: U–Pb age evidence from the Southern Variscan branch (Sardinia, Italy). *Gondwana Research*, *17*(1), 44–58. doi: 10.1016/j.gr.2009.06.001

Paquette, J. L., Ménot, R.-P., Pin, C., & Orsini, J. B. (2003). Episodic and short-lived granitic pulses in a post-collisional setting: Evidence from precise U–Pb zircon dating through a crustal cross-section in Corsica. *Chemical Geology*, *198*(1-2), 1–20. doi: 10.1016/s0009-2541(02)00401-1

Puccini, A., Xhixha, G., Cuccuru, S., Oggiano, G., Xhixha, M. K., Mantovani, F., … Casini, L. (2014). Radiological characterization of granitoid outcrops and dimension stones of the Variscan Corsica-Sardinia Batholith. *Environmental Earth Sciences*, *71*(1), 393–405. doi: 10.1007/s12665-013-2442-8

Renna, M. R., Tribuzio, R., & Tiepolo, M. (2006). Interaction between basic and acid magmas during the latest stages of the post-collisional Variscan evolution: Clues from the gabbro–granite association of Ota (Corsica–Sardinia batholith). *Lithos*, *90*(1-2), 92–110. doi: 10.1016/j.lithos.2006.02.003

Rossi, P., & Cocherie, A. (1991). Genesis of a Variscan batholith: Field, petrological and mineralogical evidence from the Corsica-Sardinia batholith. *Tectonophysics*, *195*(2-4), 319–346.

Rossi, P., Oggiano, G., & Cocherie, A. (2009). A restored section of the "southern Variscan realm" across the Corsica–Sardinia microcontinent. *Comptes Rendus Geoscience*, *341*(2-3), 224–238. doi: 10.1016/j.crte.2008.12.005

Rubatto, D., Ferrando, S., Compagnoni, R., & Lombardo, B. (2010). Carboniferous high-pressure metamorphism of Ordovician protoliths in the Argentera Massif (Italy), Southern European Variscan belt. *Lithos*, *116*(1–2), 65–76. doi: 10.1016/j.lithos.2009.12.013

Soille, P. (1999). *Morphological image analysis: Principles and applications*. New York: Springer-Verlag.

Van Achterberg, E., Ryan, C. G., Jackson, S. E., & Griffin, W. L. (2001). Data reduction software for LA-ICP-MS. In P. Sylvester (Ed.), *Laser ablation-ICPMS in the earth science* (pp. 239–243). Ottawa, Ontario, Canada.

Vernon, R. H., Johnson, S. E., & Melis, E. A. (2004). Emplacement-related microstructures in the margin of a deformed pluton: The San José tonalite, Baja California, México. *Journal of Structural Geology*, *26*(10), 1867–1884. doi: 10.1016/j.jsg.2004.02.007

Vilà, M., Fernández, M., & Jiménez-Munt, I. (2010). Radiogenic heat production variability of some common lithological groups and its significance to lithospheric thermal modeling. *Tectonophysics*, *490*(3–4), 152–164. doi: 10.1016/j.tecto.2010.05.003

Virdis, S. G. P., Oggiano, G., & Disperati, L. (2012). A geomatics approach to multitemporal shoreline analysis in western mediterranean: The case of platamona-maritza beach (Northwest Sardinia, Italy). *Journal of Coastal Research*, *28*(3), 624–640.

Wetherill, G. W. (1956). Discordant uranium-lead ages, I. *Transactions of the American Geophysical Union*, *37*, 320–326.

Wiedenbeck, M., AllÉ, P., Corfu, F., Griffin, W. L., Meier, M., Oberli, F., … Spiegel, W. (1995). Three Natural Zircon Standards for U-Th-Pb, Lu-Hf, Trace Element and Ree Analyses. *Geostandards and Geoanalytical Research*, *19*(1), 1–23. doi: 10.1111/j.1751-908X.1995.tb00147.x